

IMECE2004-60507

SYSTEM IDENTIFICATION AND OPTIMAL CONTROL OF A 6-DOF MAGNETIC LEVITATION STAGE WITH NANOPositionING CAPABILITES

Huzefa Shakir, Won-jong Kim, and Shobhit Verma
Mechanical Engineering Department
Texas A&M University
College Station 77843-3123
Phone: (979) 845-3645

ABSTRACT

A systematic procedure for modeling and optimal control of a multivariable 6-DOF (degree-of-freedom) magnetically levitated (maglev) stage has been described in this paper. In our previous publications, we have presented the design, SISO (single-input single-output) control, and testing of the maglev stage with nanometer-precision positioning capability and several-hundred-micrometer travel range. In the present work, we extended the current model to a more rigorous LQR (linear quadratic regulation) controller for the lateral control to reduce the coupling between axes. Independent lead-lag controllers have been used for the vertical control. The system equations have been derived using the Euler angle methodology and linearized about an operating point. The performance of this multivariable control has been analyzed and compared with all the six decoupled SISO controllers. The effect of adding the integrators to eliminate the steady-state error has also been discussed and the performance of the LQR controller with different weight matrices has been compared. In this paper, we also address the issues related to the stochastic modeling of the stage to analyze the coupling between different axes and transfer function identification.

KEYWORDS

Multivariable optimal control, system identification, stochastic modeling, LQR, precision positioning.

1. INTRODUCTION

Need of nanomanipulation devices is continuously increasing due to a large number of nanoscale manufacturing applications. The purpose of a nanopositioning system is to position and orient the object precisely. The required properties of a positioner are precise positioning in multiple axes

(translation and rotation), longer travel ranges, controlled at high bandwidths. This precision positioning capability along with accurate manufacturing techniques will lead to production of nanoscale objects and assemblies. The nanomanipulation systems will be capable of precisely position and orient the atomic-scale material for characterization and other operations.

The most commonly used nanopositioning devices are scanning tunneling microscopes (STMs) and atomic force microscopes (AFMs) [1-3]. However, there are several technical limitations on the application of these devices like a shorter travel range on the order of 100 μm and only planar motion capability. Most of these devices use piezoelectric devices for actuation. There are several technical difficulties with these kinds of actuators. (1) There is some hysteresis involved during the motion that influences the repeatability. (2) Thermal drift due temperature change greatly affects the accuracy. (3) The slow creeping motion after a large step causes significant positional error in the system. There are various other kind of precision positioning actuators were developed that perform really well for single axis actuation. One of such actuators was developed by Egshia, et al. [4]. This high-speed precision stage had 0.69-nm resolution in one axis using a non-resonant type ultrasonic motor.

Magnetic levitation (maglev) has become a very promising technology for future nanopositioning devices. There are a significant number of advantages of maglev technology over other technologies. Since there is no contact between the moving part and the stationary part there is no friction, i.e. there is not stick-slip and it does not need any lubricant and surface bearings for the smooth motion. This reduces the cost of manufacturing significantly. Due to absence of friction the modeling of the moving part is simple and it can be modeled as a pure mass. Since only one moving part generates all the

motions its dynamics is coupled in 6 DOFs. Thus a linear multivariable quadratic control is a natural choice to regulate the position of the platen, the moving part. Kim, et al. have designed a multivariable optimal control of a 6-DOF maglev stage with large motion capabilities [5]. Nakashima, et al. designed a servosystem for suppressing natural vibrations of a magnetic levitation system using closed-loop identification and H_∞ control theory [6]. Arreola, et al. performed LQR set-point stabilization for the control of a 3-DOF magnetic levitation system [7].

In this paper we describe the design and implementation of a multi-variable LQR for the lateral modes of a nanopositioning maglev stage. Section 2 gives a brief description of the Mechanical Design of the stage followed by Instrumentation Structure in Section 3. Stochastic modeling to identify the significant coupling between the axes has been discussed in Section 4. To apply the multi-variable control, a state space model of the platen has been developed in Section 5 by linearizing the equations of motion using Euler angle approach. Controller design and experimental results are presented in Section 6, and the conclusions and prospects for the future work have been summarized in the Section 7.

2. MECHANICAL DESIGN

An exploded view of the maglev stage developed is shown in Figure 1. The triangular part in the center called platen is the single moving part. This part has been assembled out of a solid aluminum plate that has been machined leaving the ribs on the sides to reduce the weight while maintaining the strength for higher natural frequency. The total mass of moving part is 0.2126 kg. There are three layers, an aluminum top plate, a viscoelastic damping layer, and a stainless-steel constraint layer attached on the top of platen with screws to damp the vibrations and improve stability. There are 6 sets of magnets for 6 single-axis actuators. Each set for horizontal actuator consist of 2 magnets and each vertical actuator have 1 magnet. The design description of single-axis actuators are described in Kim

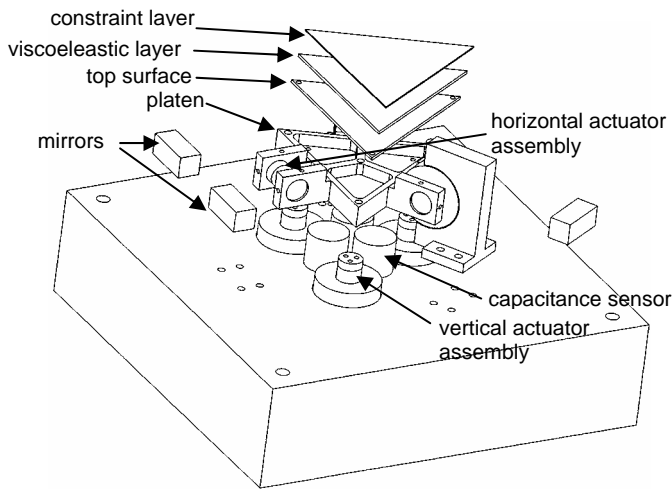


Figure 1. Exploded view of the mechanical assembly

and Maheshwari [9]. For horizontal position sensing, 3 mirrors have been mounted on the sides of the platen. These mirrors reflect the incident laser beams back to laser interferometers that give us the positional data for horizontal motions (x - and y -translation and rotation about the z -axis). For vertical motion sensing, we have 3 capacitance probes mounted on the base plate right below the platen. The detailed description of mechanical design of the stage has been given in Kim, et al. [8]. Figure 2 shows the direction of horizontal forces ($f_1, f_2,$ and f_3) and vertical forces ($f_4, f_5,$ and f_6) applied by the actuators. The combination of horizontal forces make the platen move in x, y and ϕ and combination of vertical forces make it move in z, θ and ψ [8].

3. INSTRUMENTATION STRUCTURE

The real-time digital control has been implemented on a TMS320C40 DSP (Digital Signal Processor) on a Pentek 4284 board. The job of positional data acquisition, control variable calculation and their output is done in an interrupt service routine that is called by an external interrupt at every 200 μ sec. A VME (Versa Module Eurocard) chassis has been used to install a VME PC (VMIC 7751) and 3 laser-axis boards (Agilent 10897B) along with the Pentek 4284. The C-codes are written and compiled on the VME PC and then downloaded to the DSP. A user interface has been developed that interacts with DSP for real time position inputs during the operation. This exchange on data takes place though a dual port memory on Pentek 4284. The positional data from laser axes board is available on the VME bus at a 10-MHz refresh rate at a resolution of 0.6 nm. For vertical position sensing, 3 capacitance sensing probes (ADE 2810) with signal conditioning boards (ADE 3800) have been employed. The analog outputs of these boards are fed to a data-acquisition board on VME chassis after a 1-kHz low-pass anti-aliasing filter. This data-acquisition board contains 8 channels of 16-bit ADCs (Analog to Digital converters) and 8 channels of 16-bit

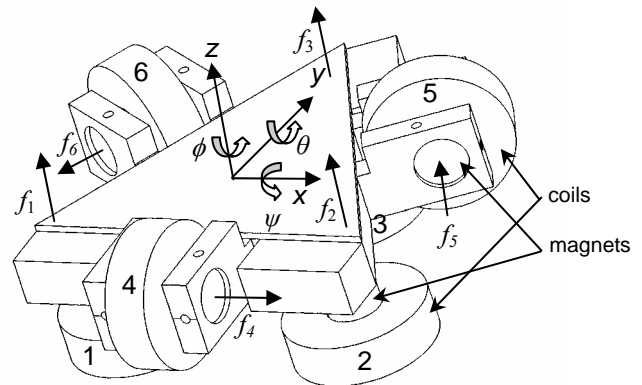


Figure 2. Forces from each unit actuator and axes convention

DACs (Digital to Analog converters) with I/O (Input/Output) range of ± 5 V. The output of the control law is given to transconductance amplifiers via DAC. The output of amplifier causes flow of desired current in the coils.

4. STOCHASTIC MODELING

In this section, we address the stochastic modeling of the plant including transfer function identification. To obtain the fast dynamics through high-bandwidth control, high system structural resonant frequency is required for system stability. Since the stage has a single moving part, it has the advantage over its counterparts with multiple moving parts since its mechanical structure is simple and can be made stiff.

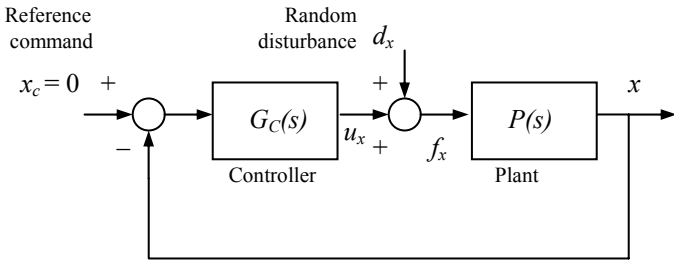


Figure 3. Block diagram for stochastic transfer function identification

Figure 3 shows the block diagram to obtain the transfer function of the plant, i.e., the levitated platen. We apply a stochastic system identification methodology that uses the force input as random disturbance. A detailed treatment of the stochastic modeling can be found in the classical texts such as [10]. The random disturbance is generated in the software with the “rand ()” function in the ANSI C language. Since the maglev system is open loop unstable, the magnitude of the random disturbance, 0.10 N, was chosen with some iterations to excite the plant persistently without losing stability [11].

The plant transfer function’s magnitude in ψ direction when the force is applied in the y direction and in the θ direction when the force is applied in the x direction has been shown in the Figure 4. These were the only significant magnitudes obtained with the experiments. The transfer function magnitudes in the other directions were significantly lower as compared with these. The reason for this coupling is due to the difference in the plane of application of lateral forces and the plane of center of mass of the platen which results in an unwanted moment about the y -axis (θ) when the force is applied in x and a moment about the x -axis (ψ) when the force is applied in y . This coupling is also confirmed by the linearized plant dynamics equation (3) given in the next section.

Also, it may be observed from the plots that the main structural resonance is at about 200 Hz for both the coupling dynamics with no other significant resonance under that frequency. Furthermore, there are no significant frequencies for the transfer function measured between x and d_x under 2.5 kHz.

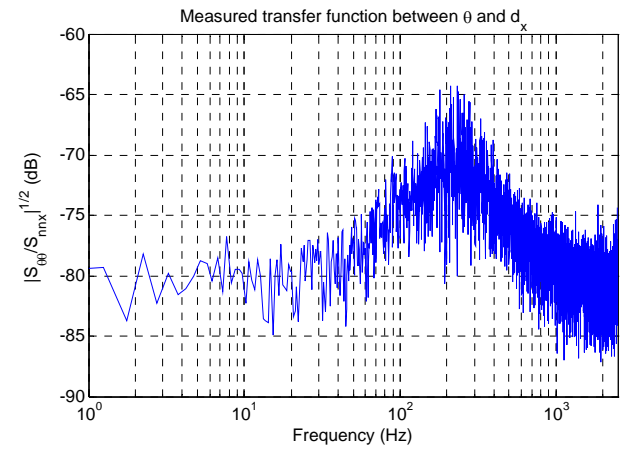
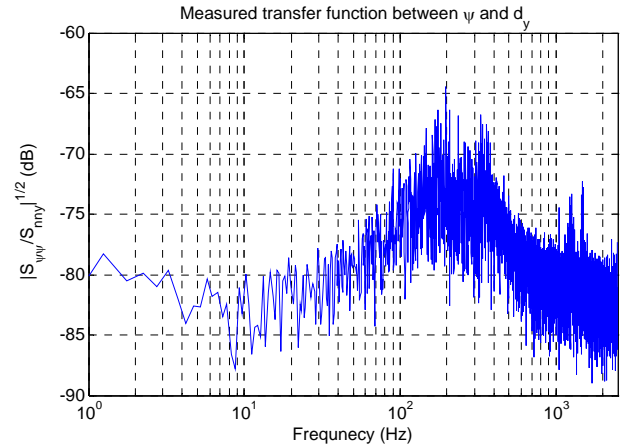


Figure 4. Measured transfer functions using stochastic modeling

This high resonant frequency could be achieved because of the simple mechanical structure of the moving platen and it allows high-bandwidth control and fast dynamics with a single moving part.

5. PLANT MODELING AND LINEARIZATION

Since the platen generates all the required motions, its dynamics is coupled in all the 6-DOFs. In order to understand the observed dynamic behavior and develop high-performance controllers, precise dynamic modeling is required. However, the previously designed decoupled SISO lead-lag controllers do not address the dynamic coupling between the axes. Thus, a multivariable linear quadratic controller is a natural choice to regulate the position of the platen. To start with, we decouple the plant into two modes – vertical and lateral – against all the six decoupled axes used previously. We design a linear quadratic regulator for the lateral modes (x , y and angle around z -axis, ϕ) and keep the decoupled SISO lead-lag controllers for the vertical modes (z , angle around x -axis, ψ and angle around y -axis, θ). The reason for this choice is that we do not need to differentiate the position data or build a state estimator for

velocity feedback, as full state feedback is provided by the laser electronics (HP10897A) for the lateral control.

To apply the multivariable control, a state-space model of the platen dynamics is required. The full equations of motion are nonlinear because of the nonlinear current-force characteristics of the coil as well as the dependence of motion of the platen on the trigonometric functions of the angles of rotation with respect to the inertial frame. We follow the xyz convention to define the Euler angles, which is commonly used in the industrial applications [12]. For small angular motions in the levitator, the Euler angles ψ , θ , and ϕ can be considered as rotational angles around x -, y -, and z -axes respectively. The state variable to describe the general motions of the platen completely in 6 DOFs may be now chosen as follows.

$$\mathbf{x} = [x \ y \ z \ u \ v \ w \ \psi \ \theta \ \phi \ p \ q \ r]^T \quad (1)$$

The first six states are the position (in m) and velocity (in m/s) components of the center of mass of the platen with respect to the origin of the inertial frame described in the inertial frame. The seventh, eighth, and ninth states are the Euler angles (in rad) and the last three states are the angular velocity (in rad/s) components of the platen described in the body frame. The angular velocity components described in the inertial frame are approximately the same as those described in the body frame in case of a small signal linearized equations of motion. Using the conservation of linear momentum in the inertial frame and Euler's equation, we get the following nonlinear equations of motion.

$$\begin{aligned} \dot{x} &= u \\ \dot{y} &= v \\ \dot{z} &= w \\ \dot{u} &= \left(\frac{1}{M}\right) \left\{ \begin{aligned} &(\cos\theta \cos\phi)(f_x) + (\sin\psi \sin\theta \cos\phi - \cos\psi \sin\phi)(f_y) \\ &+ (\cos\psi \sin\theta \cos\phi + \sin\psi \sin\phi)(f_z) \end{aligned} \right\} \\ \dot{v} &= \left(\frac{1}{M}\right) \left\{ \begin{aligned} &(\cos\theta \sin\phi)(f_x) + (\sin\psi \sin\theta \sin\phi + \cos\psi \cos\phi)(f_y) \\ &+ (\cos\psi \sin\theta \sin\phi - \sin\psi \cos\phi)(f_z) \end{aligned} \right\} \\ \dot{w} &= \left(\frac{1}{M}\right) \left\{ -\sin\theta(f_x) + \cos\theta \sin\psi(f_y) + \cos\theta \cos\psi(f_z) - g \right\} \\ \dot{\psi} &= p + \left(\frac{\sin\theta \sin\psi}{\cos\theta}\right)q + \left(\frac{\sin\theta \cos\psi}{\cos\theta}\right)r \\ \dot{\theta} &= (\cos\psi)q - (\sin\psi)r \\ \dot{\phi} &= \left(\frac{\sin\psi}{\cos\theta}\right)q + \left(\frac{\cos\psi}{\cos\theta}\right)r \\ \dot{p} &= \left(\frac{1}{I_{xx}}\right) \left\{ \begin{aligned} &\cos\theta \cos\phi(\tau_x) + (\sin\theta \sin\psi \cos\phi - \cos\psi \sin\phi)(\tau_y) \\ &+ (\cos\psi \sin\theta \cos\phi + \sin\psi \sin\phi)(\tau_z) \end{aligned} \right\} \\ \dot{q} &= \left(\frac{1}{I_{yy}}\right) \left\{ \begin{aligned} &\cos\theta \sin\phi(\tau_x) + (\sin\theta \sin\psi \sin\phi + \cos\psi \cos\phi)(\tau_y) \\ &+ (\cos\psi \sin\theta \sin\phi - \sin\psi \cos\phi)(\tau_z) \end{aligned} \right\} \\ \dot{r} &= \left(\frac{1}{I_{zz}}\right) \left\{ -\sin\theta \tau_x + \cos\theta \sin\psi \tau_y + \cos\theta \cos\psi \tau_z \right\} \quad (2) \end{aligned}$$

Using the perturbation formulae, the full state equations for small linear and angular position variations around the operating point $\mathbf{x}^* = \mathbf{0}$ for the levitator can be shown by applying Newton's second law.

$$\begin{aligned} \begin{bmatrix} \dot{\tilde{x}} \\ \dot{\tilde{y}} \\ \dot{\tilde{z}} \\ \dot{\tilde{u}} \\ \dot{\tilde{v}} \\ \dot{\tilde{w}} \\ \dot{\tilde{\psi}} \\ \dot{\tilde{\theta}} \\ \dot{\tilde{\phi}} \\ \dot{\tilde{p}} \\ \dot{\tilde{q}} \\ \dot{\tilde{r}} \end{bmatrix} &= \begin{bmatrix} 0 & 0 & 0 & 1 & 0 & 0 & 0 & 0 & 0 & 0 & 0 & 0 \\ 0 & 0 & 0 & 0 & 1 & 0 & 0 & 0 & 0 & 0 & 0 & 0 \\ 0 & 0 & 0 & 0 & 0 & 1 & 0 & 0 & 0 & 0 & 0 & 0 \\ 0 & 0 & 0 & 0 & 0 & 0 & 0 & 9.8100 & 0 & 0 & 0 & 0 \\ 0 & 0 & 0 & 0 & 0 & 0 & -9.8100 & 0 & 0 & 0 & 0 & 0 \\ 0 & 0 & 0 & 0 & 0 & 0 & 0 & 0 & 0 & 0 & 0 & 0 \\ 0 & 0 & 0 & 0 & 0 & 0 & 0 & 0 & 0 & 1 & 0 & 0 \\ 0 & 0 & 0 & 0 & 0 & 0 & 0 & 0 & 0 & 0 & 1 & 0 \\ 0 & 0 & 0 & 0 & 0 & 0 & 0 & 0 & 0 & 0 & 0 & 1 \\ 0 & 0 & 0 & 0 & 0 & 0 & 0 & 0 & -4.1670 & 0 & 0 & 0 \\ 0 & 0 & 0 & 0 & 0 & 0 & 0 & 0 & 12.2462 & 0 & 0 & 0 \\ 0 & 0 & 0 & 0 & 0 & 0 & 2.3475 & -6.3487 & 0 & 0 & 0 & 0 \end{bmatrix} \begin{bmatrix} \tilde{x} \\ \tilde{y} \\ \tilde{z} \\ \tilde{u} \\ \tilde{v} \\ w \\ \tilde{\psi} \\ \tilde{\theta} \\ \tilde{\phi} \\ \tilde{p} \\ \tilde{q} \\ \tilde{r} \end{bmatrix} \\ + \begin{bmatrix} 0 & 0 & 0 & 0 & 0 & 0 \\ 0 & 0 & 0 & 0 & 0 & 0 \\ 0 & 0 & 0 & 0 & 0 & 0 \\ 4.7037 & 0 & 0 & 0 & 0 & 0 \\ 0 & 4.7037 & 0 & 0 & 0 & 0 \\ 0 & 0 & 4.7037 & 0 & 0 & 0 \\ 0 & 0 & 0 & 0 & 0 & 0 \\ 0 & 0 & 0 & 0 & 0 & 0 \\ 0 & 0 & 0 & 7525.5870 & 0 & 0 \\ 0 & 0 & 0 & 0 & 8177.9522 & 0 \\ 0 & 0 & 0 & 0 & 0 & 4239.6235 \end{bmatrix} \begin{bmatrix} \tilde{f}_x \\ \tilde{f}_y \\ \tilde{f}_z \\ \tilde{\tau}_x \\ \tilde{\tau}_y \\ \tilde{\tau}_z \end{bmatrix} \quad (3) \end{aligned}$$

The coupling terms between vertical mode and the lateral mode comes due to the following relations:

$$\dot{\tilde{u}} = 9.81\tilde{\theta} + f(\mathbf{u}), \quad \dot{\tilde{v}} = -9.81\tilde{\psi} + f(\mathbf{u})$$

Both $\tilde{\theta}$ and $\tilde{\psi}$ have the maximum values of the order of 1.5 mrad and their influence on the velocities $\dot{\tilde{u}}$ and $\dot{\tilde{v}}$ are less than 1.5% of their values. Thus, we may neglect the effect of these coupling terms between vertical and horizontal modes, and the linearized small-signal lateral mode dynamics can be represented as follows:

$$\begin{aligned} \begin{bmatrix} \dot{\tilde{x}} \\ \dot{\tilde{y}} \\ \dot{\tilde{z}} \\ \dot{\tilde{u}} \\ \dot{\tilde{v}} \\ \dot{\tilde{r}} \end{bmatrix} &= \begin{bmatrix} 0 & 0 & 0 & 1 & 0 & 0 \\ 0 & 0 & 0 & 0 & 1 & 0 \\ 0 & 0 & 0 & 0 & 0 & 1 \\ 0 & 0 & 0 & 0 & 0 & 0 \\ 0 & 0 & 0 & 0 & 0 & 0 \\ 0 & 0 & 0 & 0 & 0 & 0 \end{bmatrix} \begin{bmatrix} \tilde{x} \\ \tilde{y} \\ \tilde{z} \\ \tilde{u} \\ \tilde{v} \\ \tilde{r} \end{bmatrix} + \begin{bmatrix} 0 & 0 & 0 \\ 0 & 0 & 0 \\ 0 & 0 & 0 \\ 4.7037 & 0 & 0 \\ 0 & 4.7037 & 0 \\ 0 & 0 & 4239.6235 \end{bmatrix} \begin{bmatrix} \tilde{f}_x \\ \tilde{f}_y \\ \tilde{f}_z \\ \tilde{\tau}_x \\ \tilde{\tau}_z \end{bmatrix} \quad (4) \end{aligned}$$

All the open loop poles are at origin and hence the plant is not open loop stable. This is because of the simple mass assumption neglecting the actuator dynamics.

6. LINEAR QUADRATIC REGULATION FOR LATERAL CONTROL

We represent the dynamic system in equation (4) as follows:

$$\dot{\mathbf{x}}(t) = A\mathbf{x}(t) + B\mathbf{u}(t). \quad (5)$$

where \mathbf{x} is the state vector and \mathbf{u} is the input vector. Define the performance index as

$$J(\mathbf{x}(\cdot), \mathbf{u}(\cdot), t_0) = \int_{t_0}^{\infty} (\mathbf{u}^T(t)R\mathbf{u}(t) + \mathbf{x}^T(t)Q\mathbf{x}(t)) dt. \quad (6)$$

This time-invariant infinite-time regulator problem is a minimization problem to find an optimal control \mathbf{u}^* to minimize J . The solution of this problem is well-known and can be found in texts on optimal control such as [14]. The optimal controller associated with the cost function defined above using $Q = \text{diag} \left(\left[\begin{array}{cccccc} 2 \times 10^6 & 2 \times 10^6 & 2 \times 10^6 & 1 \times 10^3 & 1 \times 10^3 & 1 \times 10^3 \end{array} \right] \right)$ and $R = \text{diag} \left(\left[\begin{array}{ccc} 0.1 & 0.1 & 1000 \end{array} \right] \right)$ is given by

$$K = \begin{bmatrix} 4472.14 & 0 & 0 & 109.09 & 0 & 0 \\ 0 & 4472.14 & 0 & 0 & 109.09 & 0 \\ 0 & 0 & 44.72 & 0 & 0 & 1.01 \end{bmatrix}. \quad (7)$$

where, Q and R are obtained after a few iterations, starting with using acceptable values of \mathbf{x} and \mathbf{u} such that

$$Q_{ii} = \frac{1}{\max[x_{ii}]^2}, \quad R_{ii} = \frac{1}{\max[u_{ii}]^2}$$

The corresponding closed-loop system dynamics $\dot{\mathbf{x}}(t) = (A - BR^{-1}B^T P)\mathbf{x}(t)$ is

$$\begin{bmatrix} \dot{\tilde{x}} \\ \dot{\tilde{y}} \\ \dot{\tilde{\phi}} \\ \dot{\tilde{u}} \\ \dot{\tilde{v}} \\ \dot{\tilde{r}} \end{bmatrix} = \begin{bmatrix} 0 & 0 & 0 & 1 & 0 & 0 \\ 0 & 0 & 0 & 0 & 1 & 0 \\ 0 & 0 & 0 & 0 & 0 & 1 \\ -2.10 \times 10^4 & 0 & 0 & -5.13 \times 10^2 & 0 & 0 \\ 0 & -2.10 \times 10^4 & 0 & 0 & -5.13 \times 10^2 & 0 \\ 0 & 0 & -1.90 \times 10^3 & 0 & 0 & -4.28 \times 10^3 \end{bmatrix} \begin{bmatrix} \tilde{x} \\ \tilde{y} \\ \tilde{\phi} \\ \tilde{u} \\ \tilde{v} \\ \tilde{r} \end{bmatrix}. \quad (8)$$

The closed-loop poles are placed at -4239.40 , -468.22 , -468.22 , -44.93 , -44.93 , and -44.73 , so the closed-loop system has been stabilized. Since the controller is to be implemented digitally in a 320C40 digital signal processor, we need the control gain in a discrete time domain. The discrete feedback gain is calculated with the 'lqrd' function in MATLAB with sampling rate of 5 kHz. Figure 5 shows the position, control effort required and the velocity for a 50 μm step in y -direction. It can be observed from figure 5 that there was a steady-state error of about 2 μm . This is because of the fact that the traditional LQR does not have an integrator. Thus we need to augment the controller with integrators to eliminate non-zero steady-state error. In our case, we are interested just in the position command tracking, so we use three integrators, one each for positions x , y and ϕ .

Consider, the plant defined by the following equations in state-space form

$$\dot{\mathbf{x}}_p = A_p \mathbf{x}_p + B_p \mathbf{u}_p$$

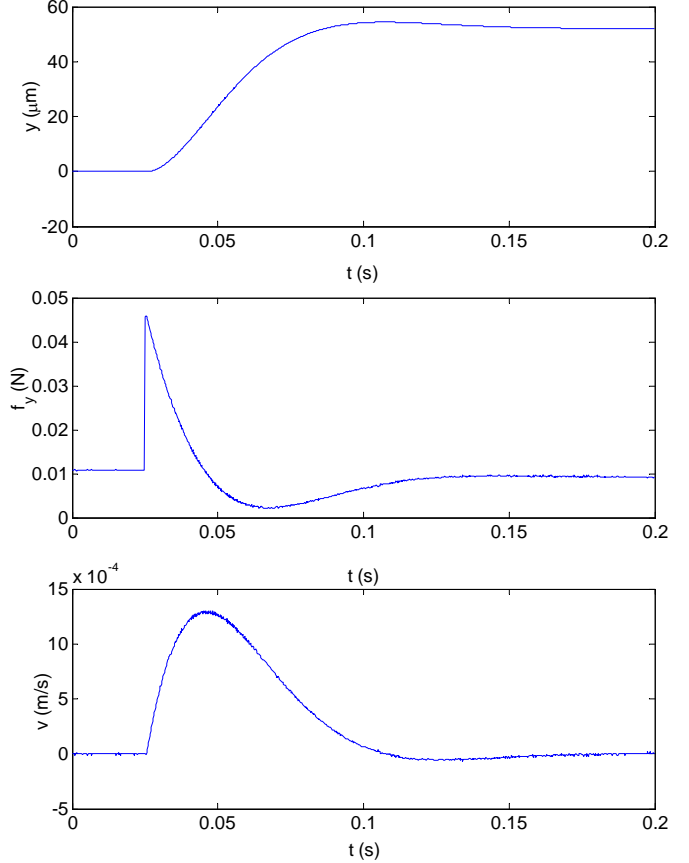


Figure 5. Step response in y -direction with LQR without integrators

$$\mathbf{y}_p = C_p \mathbf{x}_p. \quad (9)$$

Defining the new state vector ξ_p as

$$\dot{\xi}_p = \mathbf{y}_p = C_p \mathbf{x}_p,$$

we get the augmented system dynamics as:

$$\begin{bmatrix} \dot{\mathbf{x}}_p \\ \dot{\xi}_p \end{bmatrix} = \begin{bmatrix} A_p & 0 \\ C_p & 0 \end{bmatrix} \begin{bmatrix} \mathbf{x}_p \\ \xi_p \end{bmatrix} + \begin{bmatrix} B_p \\ 0 \end{bmatrix} \mathbf{u}_p$$

$$\mathbf{y}_p = \begin{bmatrix} C_p & 0 \end{bmatrix} \begin{bmatrix} \mathbf{x}_p \\ \xi_p \end{bmatrix}. \quad (10)$$

The augmented system with nine states may thus be represented as

$$\begin{bmatrix} \dot{\tilde{x}} \\ \dot{\tilde{y}} \\ \dot{\tilde{\phi}} \\ \dot{\tilde{u}} \\ \dot{\tilde{v}} \\ \dot{\tilde{r}} \\ \dot{\xi}_1 \\ \dot{\xi}_2 \\ \dot{\xi}_3 \end{bmatrix} = \begin{bmatrix} 0 & 0 & 0 & 1 & 0 & 0 & 0 & 0 & 0 \\ 0 & 0 & 0 & 0 & 1 & 0 & 0 & 0 & 0 \\ 0 & 0 & 0 & 0 & 0 & 1 & 0 & 0 & 0 \\ 0 & 0 & 0 & 0 & 0 & 0 & 0 & 0 & 0 \\ 0 & 0 & 0 & 0 & 0 & 0 & 0 & 0 & 0 \\ 0 & 0 & 0 & 0 & 0 & 0 & 0 & 0 & 0 \\ 1 & 0 & 0 & 0 & 0 & 0 & 0 & 0 & 0 \\ 0 & 1 & 0 & 0 & 0 & 0 & 0 & 0 & 0 \\ 0 & 0 & 1 & 0 & 0 & 0 & 0 & 0 & 0 \end{bmatrix} \begin{bmatrix} \tilde{x} \\ \tilde{y} \\ \tilde{\phi} \\ \tilde{u} \\ \tilde{v} \\ \tilde{r} \\ \xi_1 \\ \xi_2 \\ \xi_3 \end{bmatrix} + \begin{bmatrix} 0 & 0 & 0 \\ 0 & 0 & 0 \\ 0 & 0 & 0 \\ 4.7037 & 0 & 0 \\ 0 & 4.7037 & 0 \\ 0 & 0 & 4239.6235 \\ 0 & 0 & 0 \\ 0 & 0 & 0 \\ 0 & 0 & 0 \end{bmatrix} \begin{bmatrix} \tilde{f}_x \\ \tilde{f}_y \\ \tilde{f}_z \\ \tilde{\tau}_z \end{bmatrix}$$

$$y_p = \begin{bmatrix} 1 & 0 & 0 & 0 & 0 & 0 & 0 & 0 & 0 \\ 0 & 1 & 0 & 0 & 0 & 0 & 0 & 0 & 0 \\ 0 & 0 & 1 & 0 & 0 & 0 & 0 & 0 & 0 \end{bmatrix} \begin{bmatrix} \tilde{x} \\ \tilde{y} \\ \tilde{\phi} \\ \tilde{u} \\ \tilde{v} \\ \tilde{r} \\ \xi_1 \\ \xi_2 \\ \xi_3 \end{bmatrix}. \quad (11)$$

To analyze the effect if integrators and the weight matrices, we designed three different LQR controllers with the following set of Q and R .

$$Q = \text{diag}([2 \times 10^6 \quad 2 \times 10^6 \quad 2 \times 10^6 \quad 10^3 \quad 10^3 \quad 10^3 \quad 10^5 \quad 10^5 \quad 10^5])$$

$$R = \text{diag}([1 \quad 1 \quad 10^5]) \quad (12a)$$

$$Q = \text{diag}([2 \times 10^6 \quad 2 \times 10^6 \quad 2 \times 10^6 \quad 10^3 \quad 10^3 \quad 10^3 \quad 10^6 \quad 10^6 \quad 10^6])$$

$$R = \text{diag}([0.1 \quad 0.1 \quad 10^3]) \quad (12b)$$

$$Q = \text{diag}([10^7 \quad 10^7 \quad 10^7 \quad 10^3 \quad 10^3 \quad 10^3 \quad 10^7 \quad 10^7 \quad 10^7])$$

$$R = \text{diag}([0.1 \quad 0.1 \quad 10^3]) \quad (12c)$$

Figure 6 gives a comparison between the above three controllers. It may be observed that as we reduce the weight on R matrix, the control effort required increases. So is the case

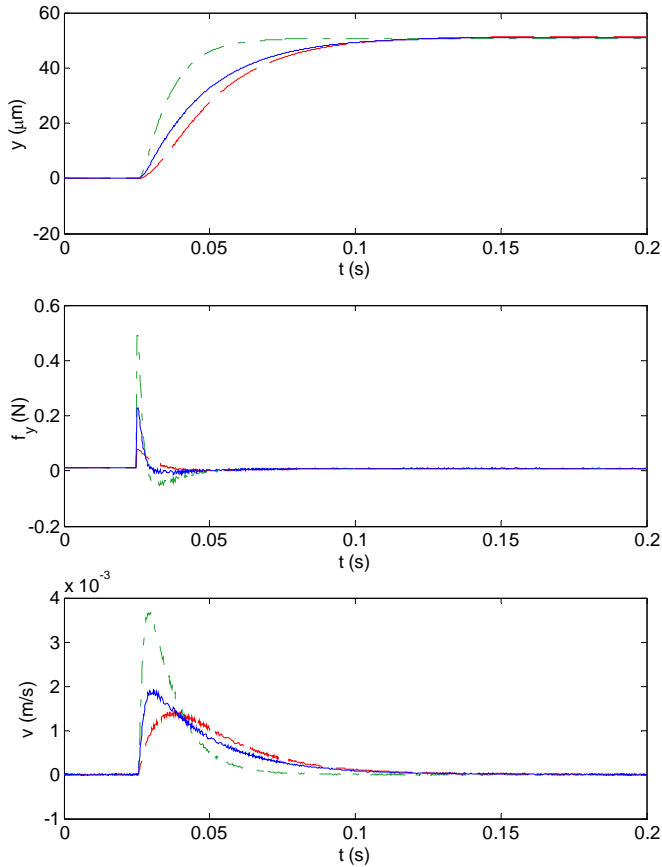


Figure 6. Comparison between three different LQR controllers; (a) dashed line, (b) solid line, (c) dash-dot line.

when we emphasize the weight on integrators since it takes larger control effort to reach the steady-state faster. Furthermore, the settling time decreases as we increase the weight on the position states but the price we have to pay appears in terms of larger control effort and higher speeds. Thus it's an optimization between the tracking and the control effort requirement, which depends on the nature of application.

Figure 7 shows the position, control effort required and the velocity for a 50 μm step in y -direction with the weight matrices given by (12b). It may be noted that with the introduction of integrators, the steady-state error has been eliminated and the dynamic performance has been improved in terms of rise time, settling time, damping and overshoot as compared with the LQR without integrators. Figure 8 shows the 50 μm step response in x - and y - and 50 μrad step response in ϕ -direction with LQR with integrators. Figure 9 shows the comparison between a 48 Hz decoupled lead-lag controller and the LQR with the weight matrices given by (12b) for a 50 μm step response in x -direction. Figure 10 shows the control effort required in the three axes and figure 11 shows the respective velocities. It may be seen that the control effort required has been substantially reduced. Also the coupling between axes has been decreased drastically. However, the dynamic performance has been affected in terms of settling time.

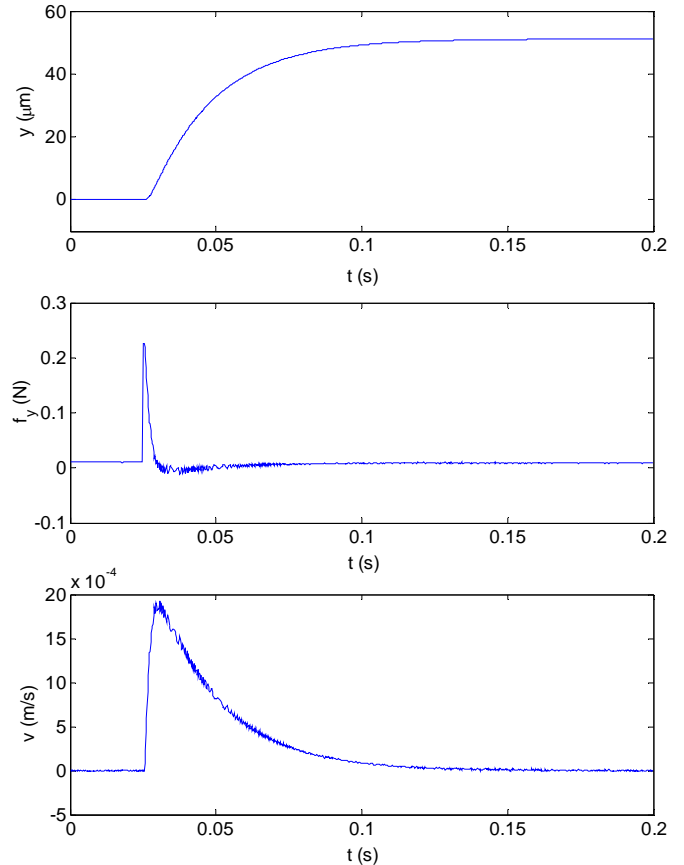


Figure 7. Step response in y -direction with LQR with integrators

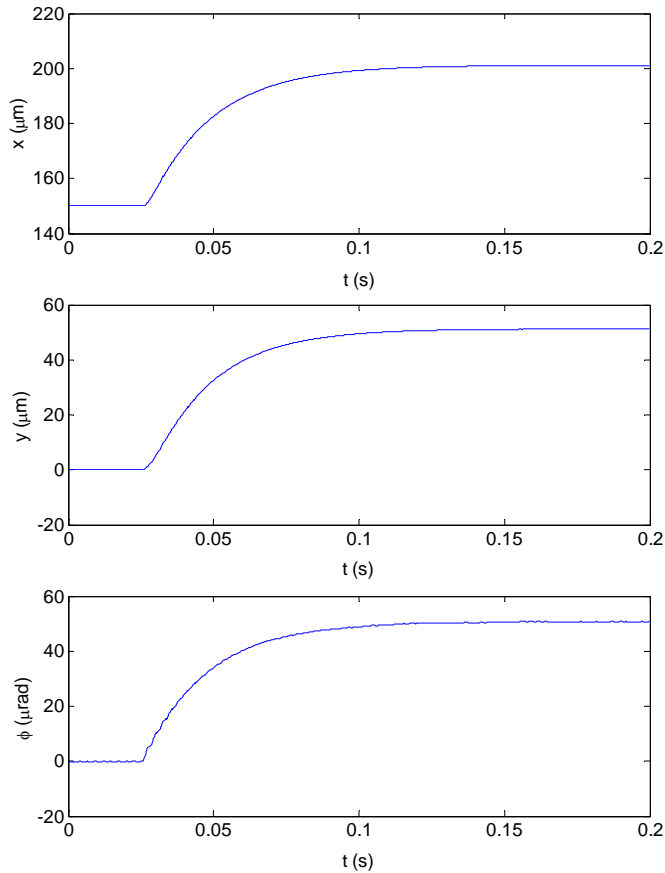


Figure 8. 50- μm step responses in x - and y - and 50- μrad step response in ϕ with LQR with integrators

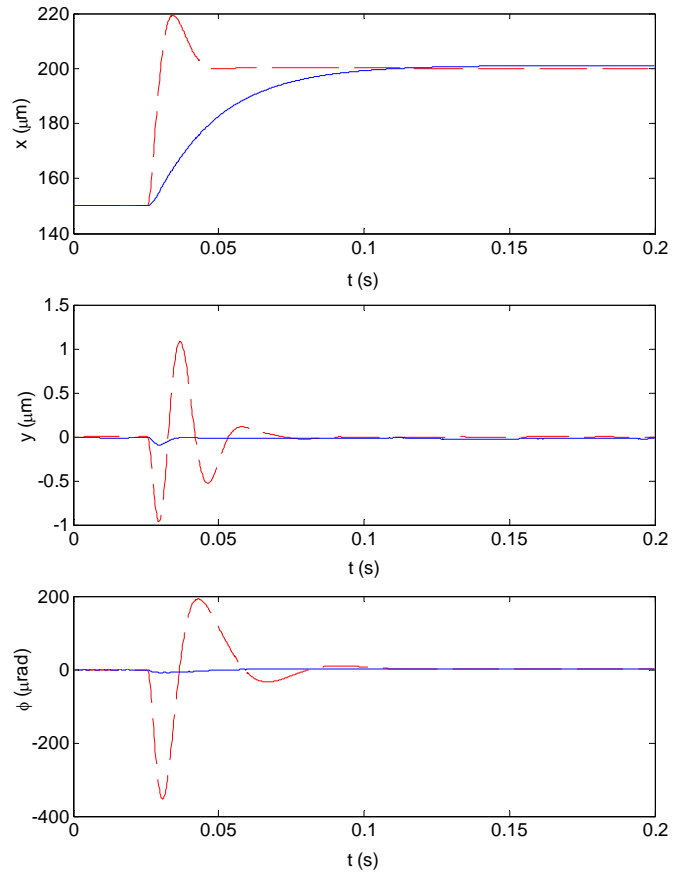


Figure 9. Step response in x with LQR with integrators; solid line: LQR, dashed line: SISO Lead-lag controller

7. CONCLUSIONS

In this paper, we present the analytical and experimental developments in a 6-DOF maglev stage with nanopositioning capabilities. Using a stochastic system identification methodology, the coupling between the axes is identified and the significant resonant frequencies are determined. The first resonant frequency for the coupled dynamics is found to be at 200 Hz with no significant frequencies for the plant dynamics less than 2.5 kHz. The coupling between the axes is confirmed by the plant linearization using the Euler angle approach and simple mass model assumption.

Since the single moving platen generates all 6-DOF motions and its dynamics is coupled among the axes, multivariable modeling and control is required to represent the plant dynamics with fidelity. A linearized plant model was developed using the plant parameters. To regulate the position, we designed and implemented a multivariable linear quadratic regulator for lateral dynamics, keeping the decoupled SISO lead-lag controllers for the vertical motion control. An augmented system has also been designed with integrators to reduce the steady-state errors in x -, y - and ϕ - directions. Step responses using the designed controllers without and with integrators have been presented and the performance of the

controllers with different weight matrices has been compared. A comparison between the multivariable LQR controller and the decoupled SISO lead-lag controllers has also been presented in terms control effort required and coupling between the axes. It turns out from the experimental results that the objectives of reduction in coupling as well as the control effort required have been met with the designed LQR controller.

ACKNOWLEDGMENTS

This material is based on the work supported by the National Science Foundation under the Grant No. CMS-00116642.

REFERENCES

- [1] Bauer, C., Bugacov, A., Koel, B. E., Madhukar, A., Montoya, N., Ramachandran, T. R., Requicha, A. A. G., Resch, R., and Will, P., 1999, "Nanoparticle Manipulation by Mechanical Pushing: Underlying Phenomena and Real-Time Monitoring," *Nanotechnology*, **9**, pp. 360–364.

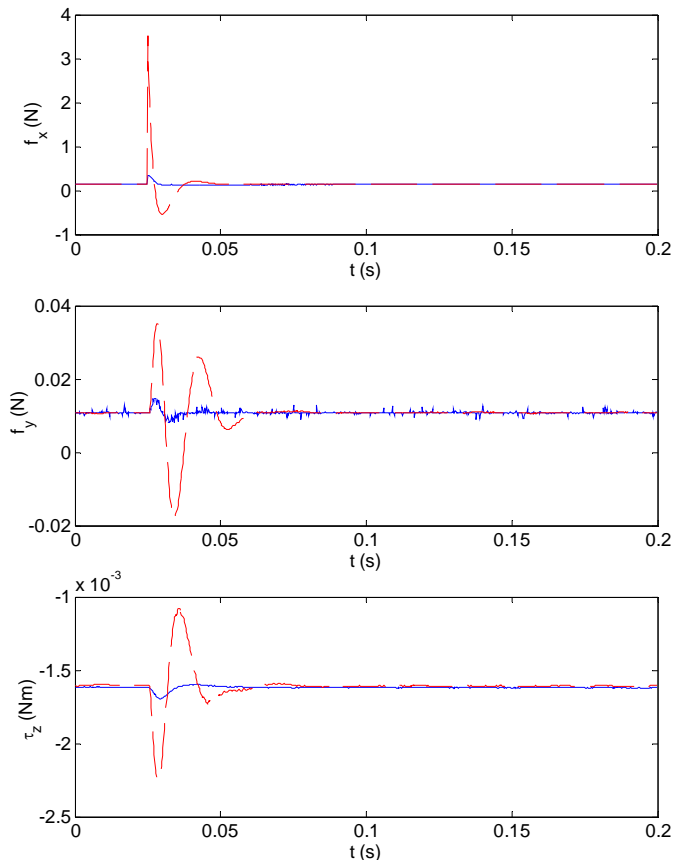


Figure 10. Control effort required for step in x with LQR with integrators; solid line: LQR controller, dashed line: SISO Lead-lag controller

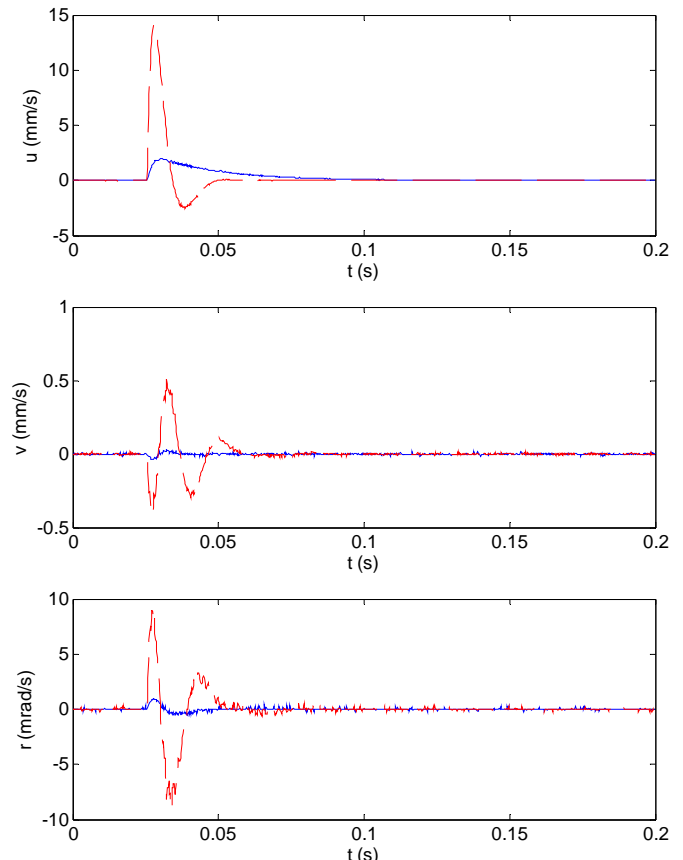


Figure 11. Lateral velocities for step in x with LQR with integrators; solid line: LQR controller, dashed line: SISO Lead-lag controller

- [2] Taylor II, R. M., 1994, "The Nanomanipulator: A Virtual-Reality Interface to a Scanning Tunneling Microscope," Ph.D. thesis, University of North Carolina, Chapel Hill.
- [3] Yu, M. F., Dyer, M. J., Rohrs, H. W., Lu, X. K., Ausman, K. D., Her, J. V., and Ruoff, R. S., 1999, "Three-Dimensional Manipulation of Carbon Nanotubes under a Scanning Electron Microscope," *Nanotechnology*, **10**, pp. 244–252.
- [4] Egshira, Y., Kosaka, K., Takada, S., Iwabuchi, T., Baba, T., Moriyama, S., Harada, T., Nagamoto, K., Nakada, A., Kubota, H., and Ohmi, T., 2001, "0.69 nm Resolution Ultrasonic Motor for Large Stroke Precision Stage," *Proceedings, IEEE-NANO 2001*, pp. 397–402.
- [5] Kim, W.J., and Trumper, D.L., 1997, "Active Multivariable Optimal Control of Planar Magnetic Levitator," *Proceedings, IEEE International Conference on Control Applications*, pp. 97–102.
- [6] Nakashima, K., Tsujino, T., and Fujii, T., 1996, "Multivariable Control of a Magnetic Levitation System using closed loop Identification and H_∞ Control Theory," *Proceedings, 35th Conference on Decision and Control*, Vol. 4, pp. 3668–3673.
- [7] Arreola, R.B., and Maggiore, M., 2002, "Modeling for Control of a Three degree-of-freedom Magnetic Levitation system," *Systems Control Group Report No. 0204*.
- [8] Verma, S., Kim, W.J., and Gu, J., 2004, "6-axis Nanopositioning Device with Precision Magnetic Levitation Technology", *IEEE/ASME Transactions on Mechatronics*, **9**, in press.
- [9] Kim, W.J., and Maheshwari, H., 2002, "High-precision control of a maglev linear actuator with nano-positioning capability," *Proceedings, American Control Conference*, pp. 4279–4284.
- [10] Maybeck, P. S., 1979, *Stochastic Models, Estimation and Control*, Academic Press.
- [11] Ljung, L., and Soderstrom, T., 1983, *Theory and Practice of Recursive Identification*, MIT Press.
- [12] Goldstein, H., 1980, *Classical Mechanics*, Addison-Wesley Publishing Co. Inc.
- [13] Kim, W.J., 1997, "High Precision Planar Magnetic Levitation," PhD thesis, Massachusetts Institute of Technology, Cambridge, MA.
- [14] Stogestad, S. and Postlewaite, I., 2003, *Multivariable Feedback Control*, John Wiley and Sons.